International Journal of Research (IJR)
P-ISSN: 2348-6848
E-ISSN: 2348-795X
Vol. 8 Issue 9
September 2021

sVehicle-to-Grid Technology in a Micro-Grid Using DC Fast Charging Architecture

Pandla Ashok Kumar[1], Dr A.Mallikarjuna Prasad[2]
[1]P.G. Scholar, [2]Guide, Principal,
[1,2], Dept. of EEE (P&ID)
[1,2] Geethanjali College Of Engineering And Technology, Kurnool
Email:- [1]kashok600@gmail.com , [2]mallikarjunaprasad0307@gmail.com

ABSTRACT

Electric Vehicle (EV) batteries can be utilized as potential energy storage devices in microgrids. They can help in micro-grid energy management by storing energy when there is a surplus (Grid-To-Vehicle, G2V) and supplying power back to the grid (Vehicle-To-Grid, V2G) when there is demand for it. Proper infrastructure and control systems have to be developed to realize this concept. Architecture for implementing a V2G-G2V system in a micro-grid using level-3 fast charging of EVs is presented in this paper. A micro-grid test system is modeled, which has a dc fast charging station for interfacing the EVs. The charging station design ensures minimal harmonic distortion of grid injected current, and the controller gives an excellent dynamic performance in dc bus voltage stability. Simulation studies are carried out to demonstrate V2G-G2V power transfer. Test results show active power regulation in the micro-grid by EV batteries through G2V-V2G modes of operation.

Keywords:- DC fast charging, Electric vehicle , Grid connected inverter , Micro-grid , Off-board charger, Vehicle-to-grid

INTRODUCTION

Up-to-date, the world has undergone a challenge in terms of providing electricity and ensuring global energy requirements. The challenge is mainly due to the shortage of primary energy resources from conventional fossil fuels like natural gas, coal, and oil. As a result, there is a great tendency to integrate renewable energy resources and the use of plug-in electric vehicles (PEVs) on the smart grid to minimize reliance on conventional energy resources, satisfy the energy demands, and consequently decreasing concerns related to global warming effects as well as the ones related to the energy crisis. Excessive electricity consumption causes intense surges in demand during peak hours, which can cause undesirable impacts and harm the stability of the existing network. That's why; some researchers are working on ways to minimize load power variance by using renewable energy sources. A stochastic multiobjective daily volt/var control based on hydro-turbine, fuel cell, wind turbine, and photovoltaic power plants is investigated. A study has developed a new control strategy that involves wind and photovoltaic generation subsystems. Energy storage systems are essential components of a micro-grid as they enable the integration of intermittent renewable energy sources.

Electric vehicle (EV) batteries can be utilized as effective storage devices in micro-grids when plugged in for charging. Most personal vehicles sit parked for about 22 hours each day, during which time they represent an idle asset. EVs could potentially help micro-

grid energy management by storing energy when there is a surplus (Grid-To-Vehicle, G2V) and feeding this energy back to the grid when there is demand for it (Vehicle-To-Grid). V2G applied to the general power grid faces some challenges such as; it is complicated to control, needs a large amount of EVs, and is hard to realize in the short term. In this scenario, it is easy to implement a V2G system in a micro-grid. The Society of Automotive Engineers defines three levels of charging for EVs. Level 1 charging uses a plug to connect the vehicle's onboard charger and a standard household (120 V) outlet. This is the slowest form of setting and works for those who travel less than 60 kilometers a day and have all night to charge. Level 2 charging uses a dedicated Electric Vehicle Supply Equipment (EVSE) at home or at a public station to provide power at 220 V or 240 V. Up to 30 A. Level three charging is also referred to as dc fast charging. DC fast-charging stations provide charging power up to 90 kW at 200/450 V, reducing the charging time to 20-30 mins. DC fast charging is preferred for implementing a V2G architecture in micro-grid due to the quick power transfer required when EVs are utilized for energy storage. Also, the dc bus can be used for integrating renewable generation sources into the system.

In the majority of the previous studies, the V2G concept has been applied in the general power grid for services like peak shaving, valley filling, regulation, and spinning reserves. The V2G development in a micro-grid facility to support power generation from intermittent renewable energy sources is still in its infancy. Also, in most of the reported works, level 1 and level 2 ac charging are utilized for V2G technology. These ac charging systems are limited by the power rating of the onboard charger. An additional issue is that the distribution grid has not been designed for bi-directional energy flow. In this scenario, there is a need to develop technically viable charging station architectures to facilitate V2G technology in micro-grids. This work proposes a dc quick charging station infrastructure with V2G capability in a micro-grid facility. The dc bus used to interface EVs is also used for integrating a solar photovoltaic (PV) array into the micro-grid. The proposed architecture allows high-power bi-directional charging for EVs through off-board chargers. The effectiveness of the proposed model is evaluated based on MATLAB/Simulink simulations for both V2G and G2V modes of operation.

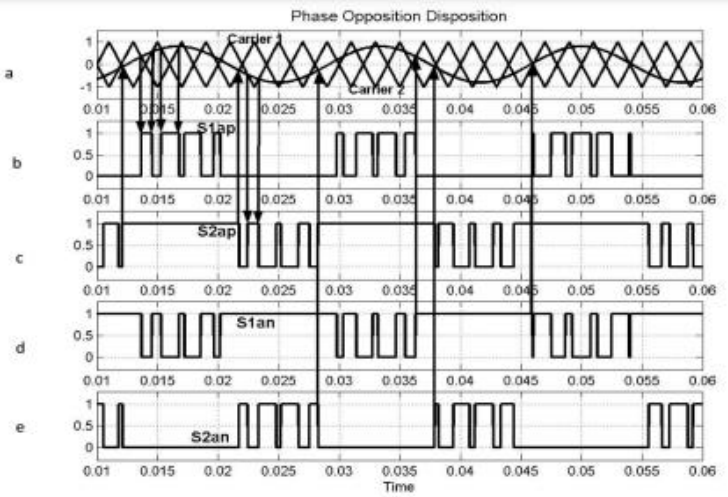

Fig. 3.8. Switching pattern produced using the POD carrier -based PWM scheme: (a) two triangles and the modulation signal (b) S1ap (c) S2ap (d) S1an (e) S2an

Phase Opposition Disposition (POD) For phase opposition disposition (POD) modulation all carrier waveforms above zero Reference are in phase and are 180out of phase with those below zero. The rules for the phase opposition disposition method, when the number of level N = 3 are (i) The N –1 = 2 carrier waveforms are arranged so that all carrier waveforms above zero are in phase and are 180 out of phase with those below zero. (ii) The converter is switched to + Vdc / 2 when the reference is greater than both carrier waveforms. (iii) The converter is switched to zero when the reference is greater than the lower carrier waveform but less than the upper carrier waveform. (iv) The converter is switched to - Vdc / 2 when the reference is less than both carrier waveforms. As seen from Fig. 3.8, the figure illustrates the switching functions produced by POD carrier-based PWM scheme. In the PWM scheme there are two triangles, upper triangle magnitude from 1 to 0 and the lower triangle from 0 to –1 and these two triangle waveforms are in out of phase. When the modulation signal is greater than both the carrier waveforms, S1ap and S2ap are turned on and the converter switches to positive node voltage and when the reference is less than the upper carrier waveform but greater than the lower carrier, S2ap and S1an are turned on and the converter switches to neutral point. When the reference is lower than both carrier waveforms, S1an and S2an are turned on and the converter switches to negative node voltage. . Fig. 3.9 shows the output voltage waveform of phase “a” and it is clear the waveform has three steps.

Alternate Phase Opposition Disposition (APOD)

In case of alternate phase disposition (APOD) modulation, every carrier waveform is in out of phase with its neighbor carrier by 180. Since APOD and POD schemes in case of three level inverter are the same, a five level inverter is considered to discuss about the APOD scheme. The rules for APOD method, when the number of level N = 5, are i) The N – 1 = 4 carrier waveforms are arranged so that every carrier waveform is in out of phase with its neighbor carrier by 180. The converter switches to + Vdc / 2 when the reference is greater than all the carrier waveforms. (ii) The converter switches to Vdc / 4 when the reference is less than the uppermost carrier waveform and greater than all other carriers. (iii) The converter switches to 0 when the reference is less than the two uppermost carrier waveform and greater than two lowermost carriers. (iv) The converter switches to - Vdc / 4 when the reference is greater than the lowermost carrier waveform and lesser than all other carriers. (v) The converter switches to -Vdc / 2 when the reference is lesser than all the carrier waveforms

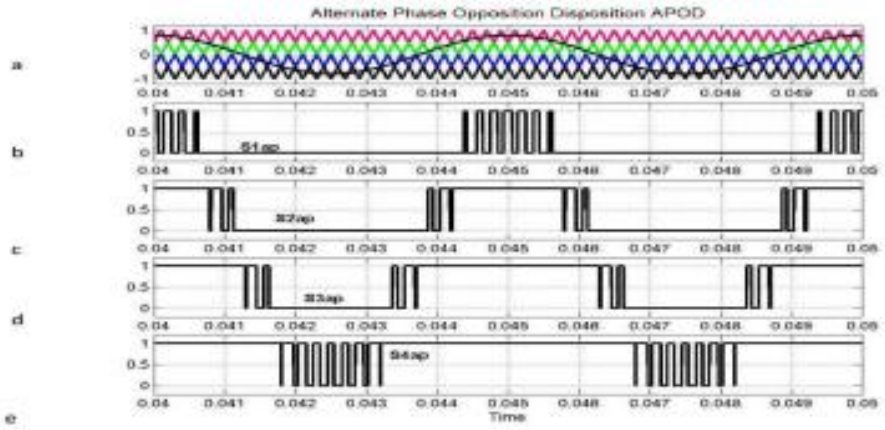

Fig. 3.10. Switching pattern produced using the APOD carrier -based PWM scheme for a five level inverter: (a) Four triangles and the modulation signal (b) S1ap (c) S2ap (d) S3ap (e) S4ap

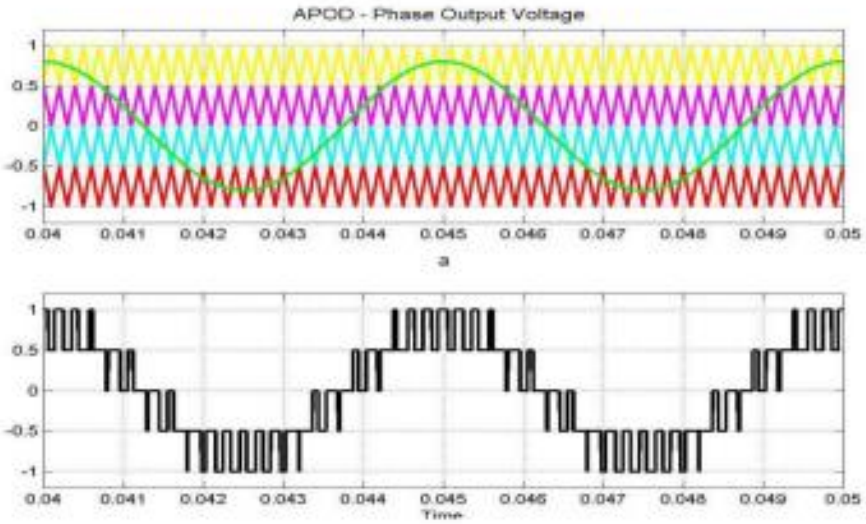

Fig. 3.11. Simulation of carrier-based PWM scheme using APOD for afive-level inverter. (a) Modulation signal and carrier waveforms (b) Phase "a" output voltage

Space vector modulation Space vector modulation (SVM) is based on vector selection in the q -d stationary reference frame. The commanded voltage vector is defined by equation -3.5. The commanded vector is plotted along with the vectors obtainable by the inverter. The desired vector V s*qds is shown at some point in time, but will follow the circular path if a three - phase set of voltages are required on the load. The first step in the SVM scheme is to identify the three nearest vectors.

Coordinate transformation: abc to dq

$$V_d = V_{an} - V_{bn}\cdot\cos 60 - V_{cn}\cdot\cos 60 = V_{an} - \frac{1}{2}V_{bn} - \frac{1}{2}V_{cn}$$

$$V_q = 0 + V_{bn}\cdot\cos 30 - V_{cn}\cdot\cos 30 = V_{an} + \frac{\sqrt{3}}{2}V_{bn} - \frac{\sqrt{3}}{2}V_{cn}$$

$$\begin{bmatrix} V_d \\ V_q \end{bmatrix} = \frac{2}{3}\begin{bmatrix} 1 & -\frac{1}{2} & -\frac{1}{2} \\ 0 & \frac{\sqrt{3}}{2} & -\frac{\sqrt{3}}{2} \end{bmatrix}\begin{bmatrix} V_{an} \\ V_{bn} \\ V_{cn} \end{bmatrix}$$

$$\left|\overline{V}_{ref}\right| = \sqrt{V_d^2 + V_q^2}$$

$$\alpha = \tan^{-1}\left(\frac{V_q}{V_d}\right) = \omega_s t = 2\pi f_s t$$

Where, f_s = fundamental frequency

Switching time duration at Sector 1 is described below

$$\int_0^{T_z}\overline{V}_{ref} = \int_0^{T_1}\overline{V}_1 dt + \int_{T1}^{T_1+T_2}\overline{V}_2 dt + \int_{T_1+T_2}^{T_z}\overline{V}_0$$

$$T_z\cdot\overline{V}_{ref} = (T_1\cdot\overline{V}_1 + T_2\cdot\overline{V}_2)$$

$$T_z\cdot\left|\overline{V}_{ref}\right|\cdot\begin{bmatrix}\cos(\alpha)\\ \sin(\alpha)\end{bmatrix} = T_1\cdot\frac{2}{3}\cdot V_{dc}\cdot\begin{bmatrix}1\\0\end{bmatrix} + T_2\cdot\frac{2}{3}\cdot V_{dc}\cdot\begin{bmatrix}\cos(\pi/3)\\ \sin(\pi/3)\end{bmatrix}$$

where $0 \le \alpha \le 60^\circ$

$$T_1 = T_z\cdot a\cdot\frac{\sin(\pi/3-\alpha)}{\sin(\pi/3)}$$

$$T_2 = T_z\cdot a\cdot\frac{\sin(\alpha)}{\sin(\pi/3)}$$

$$T_0 = T_z - (T_1 + T_2), \quad \left(\text{where,} \quad T_z = \frac{1}{f_s} \quad \text{and} \quad a = \frac{\left|\overline{V}_{ref}\right|}{\frac{2}{3}V_{dc}}\right)$$

Switching time duration at any Sector is shown below

$$T_1 = \frac{\sqrt{3}T_z\cdot|\overline{V}ref|}{V_{dc}}\left(\sin\left(\frac{\pi}{3} - \alpha + \frac{n-1}{3}\pi\right)\right) = \frac{\sqrt{3}\cdot T_z\cdot|\overline{V}ref|}{V_{dc}}\left(\sin\frac{n}{3}\pi - \alpha\right)$$

$$= \frac{\sqrt{3}\cdot T_z\cdot|\overline{V}ref|}{V_{dc}}\left(\sin\frac{n}{3}\pi\cos\alpha - \cos\frac{n}{3}\pi\sin\alpha\right)$$

$$T_2 = \frac{\sqrt{3}\cdot T_z\cdot|\overline{V}ref|}{V_{dc}}\left(\sin\left(\alpha - \frac{n-1}{3}\pi\right)\right)$$

$$= \frac{\sqrt{3}\cdot T_z|\overline{V}ref|}{V_{dc}}\left(-\cos\alpha\cdot\sin\frac{n-1}{3}\pi + \sin\alpha\cdot\cos\frac{n-1}{3}\pi\right)$$

$$T_0 = T_z - T_1 - T_2$$

Where, n=1 through 6 (that is sector 1 to 6),$0 \le \alpha \le 60^\circ$

SIMULATION RESULTS

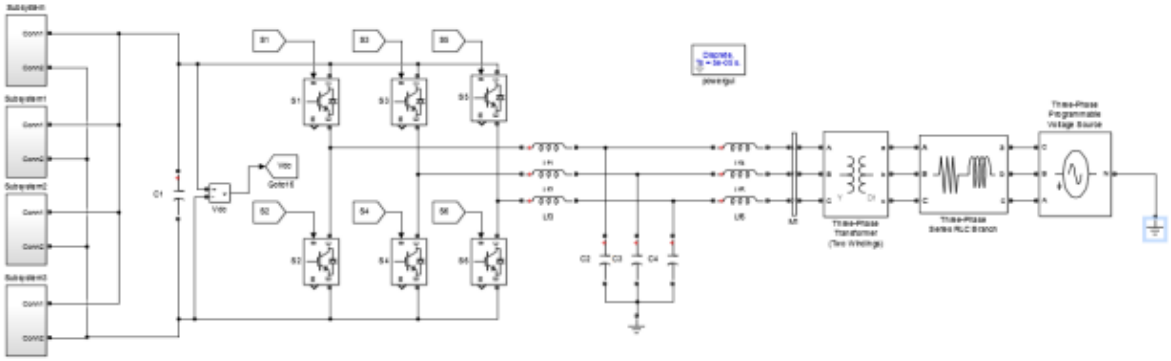

Fig. 6.1. Block diagram

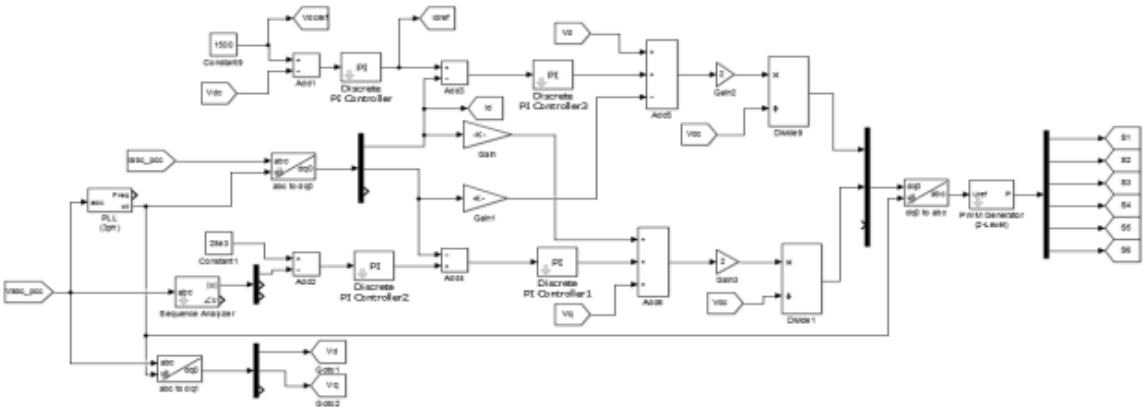

Fig. 6.2. Control scheme diagram

The charging station design procedure is adapted from and the obtained parameter values are given in Appendix. The wind turbine is operated at rated speed giving an output maximum power of 100 kW. The solar PV is operated at standard test conditions (1000W/m2 irradiance and 25o C temperature) giving the maximum power output of 50 kW. A 150 kW resistive load is connected to the 480 V ac bus. The reactive current reference to GCI is set to zero for unity pf operation. The initial state of charge (SOC) of the EV batteries is set at 50%. Once the steady state conditions are reached, batteries of EV1 and EV2 (Fig. 6.1) are operated to perform the V2G-G2V power transfer. The current set-points given to the battery charging circuits of EV1 and EV2 batteries are shown in Table I and the results are shown in the subsequent figures. The battery parameters when EV1 is operating in V2G mode and EV2 operating in G2V mode are shown in Figs. 6.3 and 6.4, respectively

P-ISSN: 2348-6848
E-ISSN: 2348-795X
Vol. 8 Issue 9
September 2021

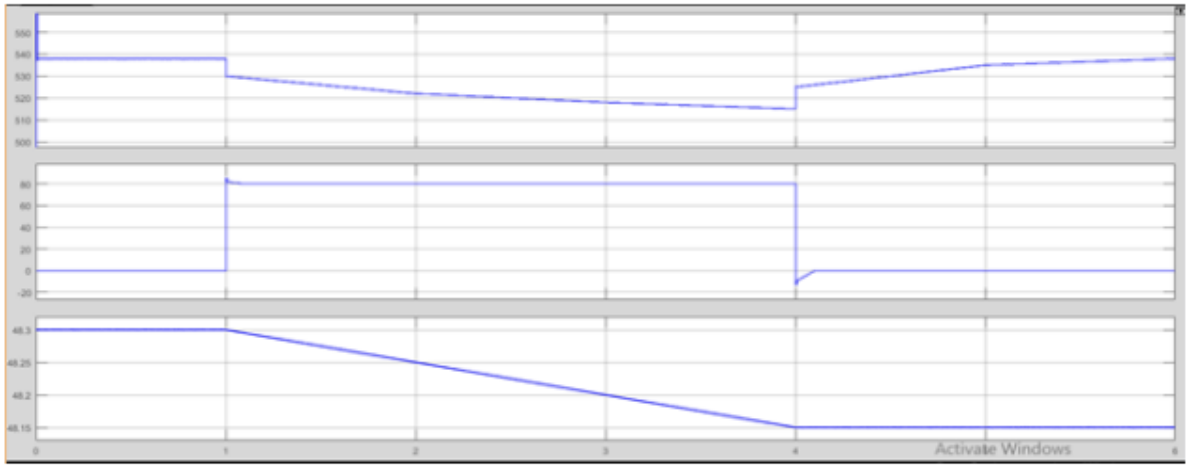

Fig. 6.3. Voltage, current, and SOC of EV1 battery during V2G operation

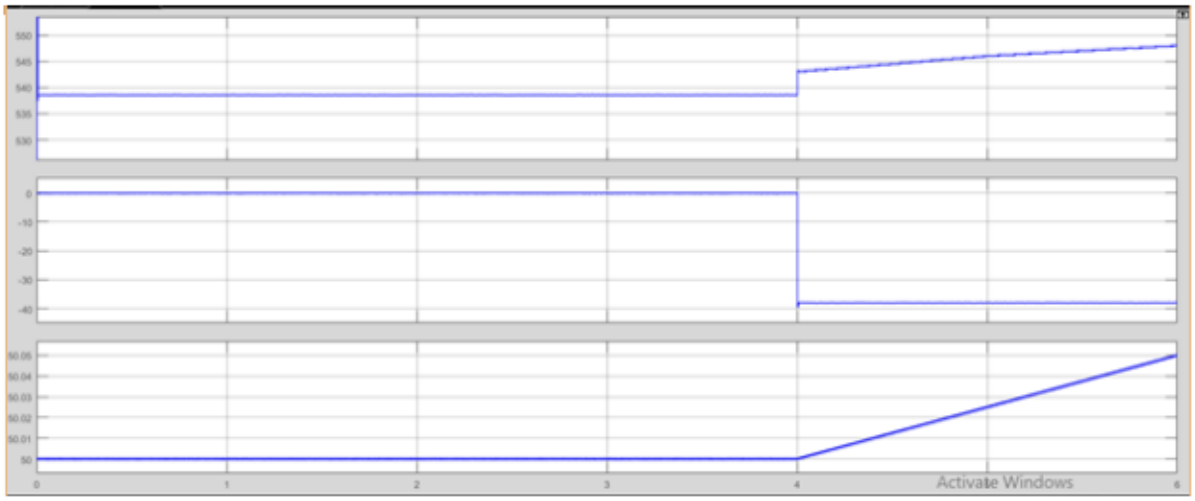

Fig. 6.4. Voltage, current, and SOC of EV2 battery during G2V operation

Fig. 6.6. Variation in dc bus voltage

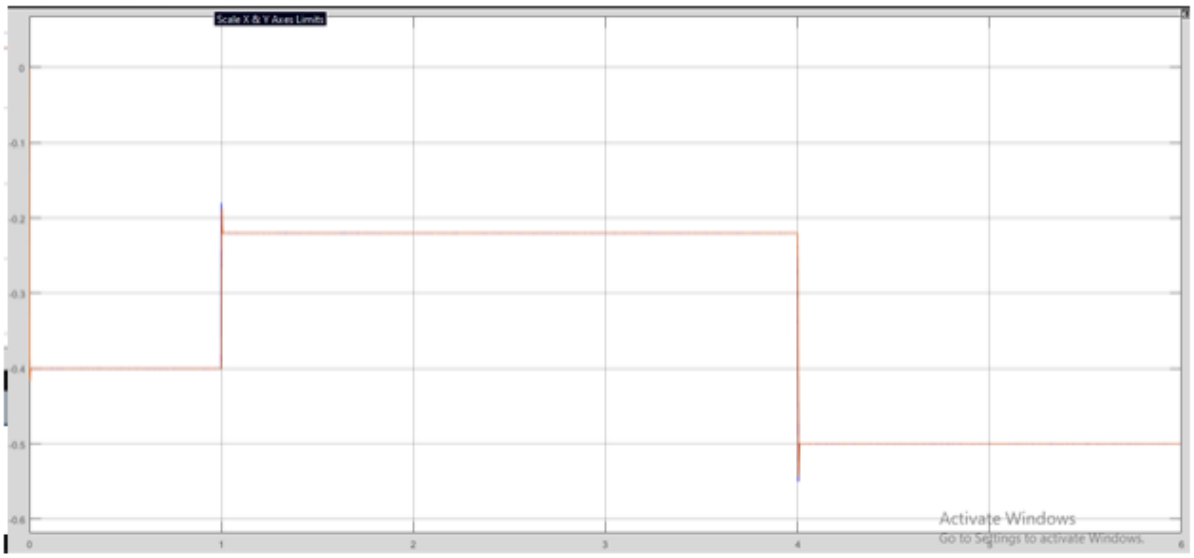

Fig. 6.7. Reference current tracking by inverter controller

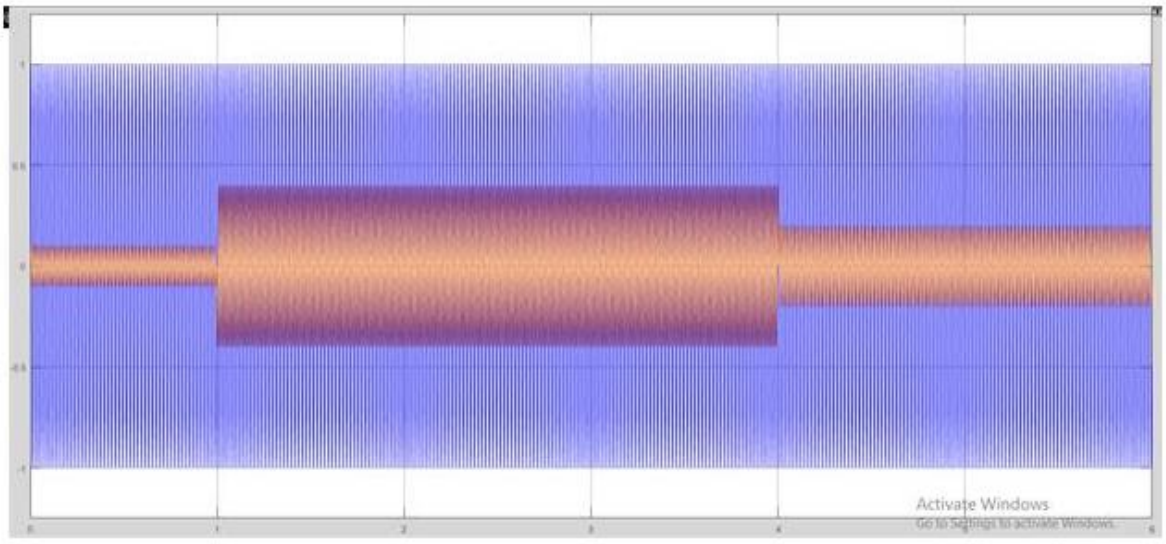

Fig. 6.8. Grid voltage and grid injected current during V2G-G2V operation

8. The grid power changes to accommodate the power transferred by the EVs. The negative polarity of the grid power from 1s to 4s shows that the power is being fed to the grid from the vehicle. The change in polarity of grid power at 4s shows that the power is supplied by the grid for charging the vehicle battery. This demonstrates the V2G-G2V operation. Also, the net power at PCC is zero showing an optimal power balance in the system The dc bus voltage is regulated at 1500 V by the outer voltage control loop of the inverter controller and is shown in Fig. 6.6. This in turn is achieved by the inner current control loop tracking the changed d-axis reference current as shown in Fig. 6.7. The grid voltage and current at PCC are shown in Fig. 6.8. Voltage and current are in phase during G2V operation and out of phase during V2G operation showing the reverse power flow Total harmonic distortion (THD) analysis is done on the grid injected current and the result is shown in Fig. 12. According to IEEE Std. 1547, harmonic current distortion on power systems 69 kV and

below are limited to 5% THD. The THD of grid injected current is obtained as 2.31 % and is achieved by the judicious design of LCL filter

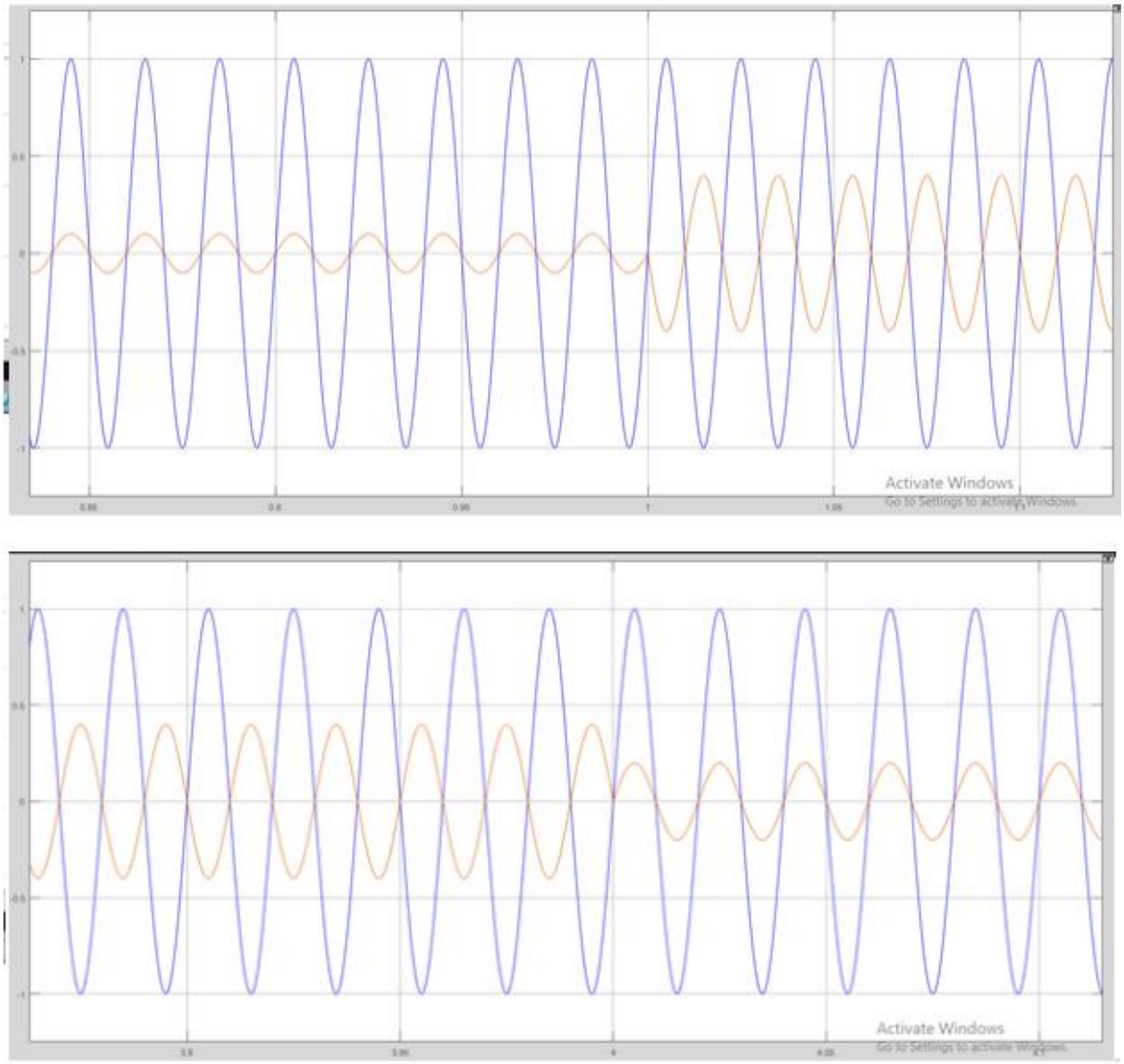

Fig. 6.9. V2G-G2V Operation

CONCLUSION

Modeling and design of a V2G system in a micro-grid using dc fast charging architecture is presented in this paper. A dc fast charging station with off-board chargers and a grid connected inverter is designed to interface EVs to the microgrid. The control system designed for this power electronic interface allows bi-directional power transfer between EVs and the grid. The simulation results show a smooth power transfer between the EVs and the grid, and the quality of grid injected current from the EVs adheres to the relevant standards. The designed controller gives good dynamic performance in terms of dc bus voltage stability and in tracking the changed active power reference. Active power regulation aspects of the microgrid are considered in this work, and the proposed V2G system can be utilized for several other services like reactive power control and frequency regulation. Design of a

supervisory controller which gives command signals to the individual EV charger controllers is suggested for future research.

REFERENCES

[1] C. Shumei, L. Xiaofei, T. Dewen, Z. Qianfan, and S. Liwei, "The construction and simulation of V2G system in micro-grid," in Proceedings of the International Conference on Electrical Machines and Systems, ICEMS 2011, 2011, pp. 1–4.
[2] S. Han, S. Han, and K. Sezaki, "Development of an optimal vehicle-togrid aggregator for frequency regulation," IEEE Trans. Smart Grid, vol. 1, no. 1, pp. 65–72, 2010.
[3] M. C. Kisacikoglu, M. Kesler, and L. M. Tolbert, "Single-phase on-board bidirectional PEV charger for V2G reactive power operation," IEEE Trans. Smart Grid, vol. 6, no. 2, pp. 767–775, 2015. [4] A. Arancibia and K. Strunz, "Modeling of an electric vehicle charging station for fast DC charging," in Proceedings of the IEEE International Electric Vehicle Conference (IEVC), 2012, pp. 1–6.
[5] K. M. Tan, V. K. Ramachandaramurthy, and J. Y. Yong, "Bidirectional battery charger for electric vehicle," in 2014 IEEE Innovative Smart Grid Technologies - Asia, ISGT ASIA 2014, 2014, pp. 406–411.